JOURNAL OF Applied Polymer SCIENCE

Improving the Oxygen Barrier Properties of Polyethylene Terephthalate by Graphite Nanoplatelets

Ahmad Al-Jabareen,[1,2] Hammam Al-Bustami,[3] Hannah Harel,[1] Gad Marom[1]

[1]Casali Institute of Applied Chemistry, The Institute of Chemistry and the Center for Nanoscience and Nanotechnology, The Hebrew University of Jerusalem, 91904 Jerusalem, Israel

[2]Materials Engineering Department, Al-Quds University, 20002 East Jerusalem, Palestine

[3]Department of Advanced Materials Engineering, The Jerusalem College of Engineering, 91035 Jerusalem, Israel

Correspondence to: H. Harel (E-mail: hannahh@savion.huji.ac.il)

ABSTRACT: Enhancement of the oxygen gas barrier properties of polyethylene terephthalate (PET), used in the packaging industry, is the main objective here. For this purpose, nanocomposites of PET containing graphite nanoplatelets (GNPs) were prepared by melt compounding. The effects of the nanocomposites' structural morphology on oxygen gas permeability were analyzed using a range of thermal, microscopic, and mechanical characterization techniques. The investigated nanocomposite films exhibited GNP exfoliated morphology and good mixing with PET, as well as uniform dispersion within the polymer. All nanocomposite films were shown to possess superior oxygen barrier properties and improved thermal and dimensional stability compared with the plain PET films. In the best case, for 1.5 wt % GNP, the oxygen permeation was reduced by more than 99%. The improved barrier properties are attributed to the direct effect of the GNPs and to their induced increase of degree of crystallinity. © 2012 Wiley Periodicals, Inc. J. Appl. Polym. Sci. 000: 000–000, 2012

KEYWORDS: composites; films; polyesters

Received 3 May 2012; accepted 4 July 2012; published online
DOI: 10.1002/app.38302

INTRODUCTION

In the packaging industry, the use of metal and glass is increasingly being replaced by plastics for applications where high barrier properties are required to prevent gases such as oxygen, carbon dioxide, and water vapor from permeating through the packaging materials, a phenomenon which can significantly decrease the shelf life of stored beverages and food products. Plastics, however, are inherently permeable to various gases and therefore, research into developing new and improved barrier property plastics has widely escalated. Consumer demands driving this escalation include lighter and thinner packaging, transparency, environmental awareness, convenience and a greater desire for fresher food products.

Polyethylene terephthalate (PET) has been extensively used in the packaging of drinking water, carbonated soft drinks, isotonic "sports" drinks and similar products over the past 20 years.[1] However, there is a continuing practical need to improve the PET barrier properties, which has been achieved in part by blending PET with high barrier polymers such as ethylene vinyl alcohol copolymer (whose excellent gas barrier properties are limited to dry environments) and semiaromatic polyamides.[2,3]

Crystallization and molecular orientation are two approaches to gas barrier enhancement. Crystallization reduces the volume fraction of the permeable amorphous phase available for gas transport, thus reducing the permeability by decreasing the total free volume in the polymer.[4–7] Similarly, molecular orientation, even without crystallization, increases the density of the amorphous phase, thereby reducing the permeability. PET, however, is an exception to the rule in that its amorphous phase might dedensify during crystallization, thereby increasing the permeability of the amorphous phase and mitigating to some extent the beneficial effects of orientation and crystallization.[8–10]

Copolymerization of PET offers another approach to enhancing its barrier properties. The gas permeability of aromatic polymers and copolymers consistently decreases when the para-phenylene linkage is replaced by a meta- or ortho-linkage.[11] This trend has been demonstrated[12–18] for various polysulfones, polyimides, polyesters, and poly(phenolphthalein phthalates). Chain symmetry appears to affect both the thermodynamic (solubility) and kinetic (diffusivity) components of permeability.

Preparation of PET-based nanocomposites by using nanofillers such as carbon nanotubes,[19,20] graphene, exfoliated graphite nanoplatelets

(GNPs),[21–24] clay,[25,26] and silica[27] improves its physical properties. Among those nanofillers, graphene has been considered recently as an ideal reinforcing material to enhance the thermal, mechanical, and electrical performances due to its outstanding thermal stability, mechanical modulus, and in-plane electrical conductivity, derived from its two-dimensional monolayer of sp^2-bonded carbon atoms arranged in a honeycomb network.[28] Yet, to the best of our knowledge, barrier properties of PET/exfoliated GNPs nanocomposites have not been investigated thoroughly.

In this study, we attempted to reduce oxygen permeability in PET by preparing a series of nanocomposites films based on PET and exfoliated GNPs via melt-mixing and molding. Then, barrier properties, morphological features, thermal properties, thermal stability, and mechanical properties were characterized.

EXPERIMENTAL

Materials and Sample Preparation

PET copolymer based on isophthalic acid (2.3%), with an intrinsic viscosity of 0.80 dL/g (in 1,1′,2,2′-tetrachloroethane/phenol, 60/40 wt %/wt %, at 25°C) and melt flow index of 19.1 g/10 min (at 260°C, 1.2 kg, according to American Society for Testing and Materials (ASTM) standard test D 1238), was used as the raw material. Exfoliated graphite nanoplatelets (GNPs) (prepared according to the method described earlier[29]) were provided by Prof. J.K. Kim of HKUST. The original thickness and diameter of the GNPs were estimated to be 4.5 nm and 46 μm, respectively, on average.[30]

The nanocomposites were prepared from precompounded PET/GNP granules (a weighed quantity of GNPs was sandwiched between two PET films and hot pressed and caged in the polymer and then chopped to granules.) by melt compounding using a twin-screw microcompounder (DSM, Netherlands) at 260°C for 5 min at a rotational speed of 100 rpm. The polymer was processed with GNPs at different concentrations: 0.1, 0.5, 1.0, and 1.5% by weight. For comparison, neat PET (ref.) was processed under the same conditions adopted for the nanocomposites.

The mixed material was compression molded into thin films with a thickness of 0.17 mm in a hot press under 17 MPa at 260°C for 5 min, then removed from the press and left to cool to room temperature. To prevent hydrolytic degradation during processing, all the materials were dried in a vacuum oven for 4 h at 120°C prior to extrusion and/or compression molding.

Samples of neat PET for thermoanalysis were prepared in similar conditions as above; one of the films was quenched in ice water immediately after pressing [PET (quenched)], and two other samples were annealed in an oven at 180 and 240°C [PET (180°C)] and [PET (240°C)], to achieve different degrees of crystallinity.

Characterization

The gas barrier properties were represented by the oxygen transmission rate (OTR). (OTR is the steady state rate at which oxygen gas permeates through a film at specified conditions of temperature and relative humidity; values are expressed in cc/m/24 h in metric (or SI) units; standard test conditions are 23°C (73 F) and 0% RH). Here the OTR was measured with a 8000 Oxygen Permeation Analyser (Systech Instruments, UK), operated according to ASTM D 3985, at 25°C, under 1 atm pressure and 0% relative humidity by using high purity nitrogen gas as the carrier gas (purity: >99.999%) and high purity oxygen gas as the testing gas (purity: >99.9%). The values, in cc/m^2/day/atm, were obtained normalizing to a film thickness of 0.17 mm. One film was tested for each composition.

Differential scanning calorimetry (DSC) (Mettler 822^e Toledo, Switzerland) thermograms were measured in a heating/cooling cycle in the temperature range 30–270°C at a heating rate of 10°C/min under a nitrogen flux of 50 mL/min. The weight of each sample was approximately 10–15 mg. The glass transition temperature (T_g) was detected from the deflection point in the heat capacity trace; the solid phase crystallization (T_{cc}) and the melting (T_m) temperatures were determined from the respective exothermal and endothermal peaks. The degrees of crystallinity (X_c) of the films were calculated from the enthalpies of the respective thermal transitions according to the following expression:

$$X_c = \frac{\Delta H_m - \Delta H_{cc}}{(1-\phi)\Delta H_f^0} \times 100\%$$

where ΔH_m is the enthalpy of the final melting and ΔH_{cc} is the enthalpy of the solid phase crystallization process, ϕ is the weight fraction of graphite in the composites, and $\Delta H_f^0 = 135.8$ J/g[31] is the heat of fusion of 100% crystallinity. The crystallization temperature from the melt (T_c) was determined from the cooling cycle.

Thermal stability of the materials was investigated by thermo gravimetric analysis (TGA) using a thermobalance analyzer (Mettler Toledo TG50), from ambient temperature to 600°C at a programmed heating rate of 10°C/min in nitrogen. A sample weight of ~10 mg was taken for all the measurements. The weight loss against temperature was recorded. The data points denote the weight loss against temperature at the specified heating rate. At least five samples were tested for each film composition.

High resolution scanning electron microscopy HRSEM (Sirion 200, FEI) was used to study the morphology of fracture surfaces. The specimens were obtained from the tensile test specimens by cryogenic fracture along the length axis. Gold-coated surfaces were viewed at right angles to the surface plane.

Tensile tests to determine the tensile strength and modulus of the nanocomposites were performed according to ASTM D638 using a universal testing machine (Instron 4502, England) at a crosshead speed of 10 mm/min. The dimensions of the rectangular press-molded tensile specimens were 60, 10, and 0.15 mm. The values reported were the averages of seven measurements.

RESULTS AND DISCUSSION

Oxygen Permeability

The results of the oxygen transmission rate (OTR) measurements and the respective degrees of crystallinity (determined by thermal analysis—see below) are given in Table I for neat PET and PET/GNP films. The first four rows of the table display

Table I. Barrier Properties and Crystallinity of Neat PET and PET/GNP Nanocomposites

Material	OTR (cc/m^2/day/atm)	X_c (%)
PET (quenched)	16.1	5.5
PET (180 °C)	8.3	23.6
PET (240 °C)	10.0	19.4
PET (ref.)	11.1	13.2
PET/GNP 0.1%	11.2	13.7
PET/GNP 0.5%	13.1	16.6
PET/GNP 1.0%	2.7	14.8
PET/GNP 1.5%	0.1	17.3

results of neat PET films prepared under different compression molding conditions in order to generate different degrees of crystallinity. It is evident that the highest OTR value by far was obtained for the quenched sample due to its lower degree of crystallinity, as listed in Table I. The decrease in OTR as a function of the degree of crystallinity is presented graphically in Figure 1 for the neat PET films, showing a linear behavior with a correlation coefficient (r) of 0.97. The composite films—prepared under the same compression molding conditions as the PET sample (260°C)—exhibit two opposing trends with the GNP content, wherein the OTR decreases with increased GNP content and the degree of crystallinity increases. These trends are presented graphically in Figure 2 where—for general impression—both are fitted with linear regression lines, exhibiting relatively good correlation coefficients (0.89 and 0.79). As seen from Figures 1 and 2, the oxygen permeability is reduced both by the presence of GNP and by degree of crystallinity.

In general, the oxygen barrier values for the PET/GNP films, as seen in Figure 2, are quite encouraging. It is evident that all of the nanocomposite films have considerably enhanced oxygen barrier properties when compared with neat PET films. The results indicate clearly that the GNPs have a two-fold effect on oxygen permeability, generated simultaneously by their inherent barrier properties and by inducing higher degrees of crystallinity.[32] Regarding the inherent barrier properties of GNPs, it has been shown in the literature that gas permeability through a

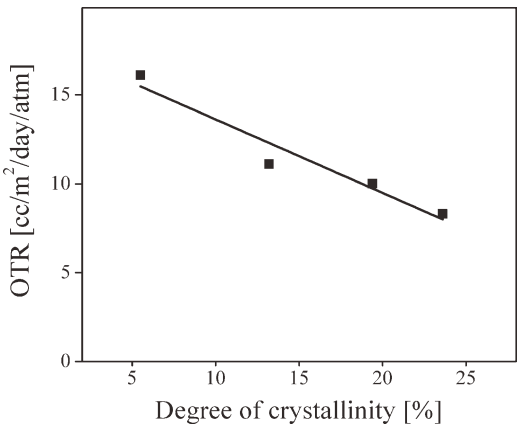

Figure 1. OTR as a function of the degree of crystallinity in neat PET.

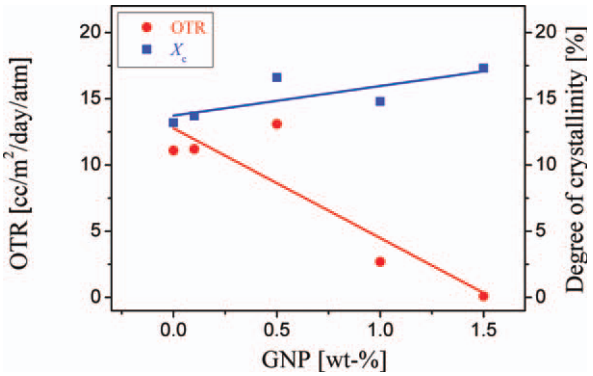

Figure 2. OTR and degree of crystallinity as a function of GNP content in composite films. [Color figure can be viewed in the online issue, which is available at wileyonlinelibrary.com.]

polymer filled with high aspect-ratio impermeable flakes can be decreased substantially via a reduced cross section for gas diffusion and a tortuous path mechanism.[33] All in all, the potential of the PET/GNP films in oxygen barrier applications to outperform those of neat PET is noticeably evident and in the best case, for 1.5 wt-% GNP, the oxygen permeation was reduced by more than 99%. This reduction is generally much higher than those reported in studies dealing with barrier properties of other types of nanocomposites, as reported in a recent perspective article.[28]

Thermal Characterization

Studying the thermal behavior of the films is essential for monitoring their thermal stability and for understanding the capability of the GNPs to nucleate and crystallize the polymer. Figure 3 presents the heating scan of DSC traces of PET samples and PET/GNP nanocomposites. Two of the main phase transition temperatures can be seen: The solid-state crystallization temperature, T_{cc}, and the melting point, T_m. Table II presents the corresponding thermal data. The neat PET sample has a T_{cc} of 129 °C, a T_m of 250 °C and a degree of crystallinity X_c of 13.2%. The main effects in the presence of GNPs are that X_c shifts to higher values (Table I), T_{cc} decreases with GNP concentration while T_m remains unaffected. These observations are compatible

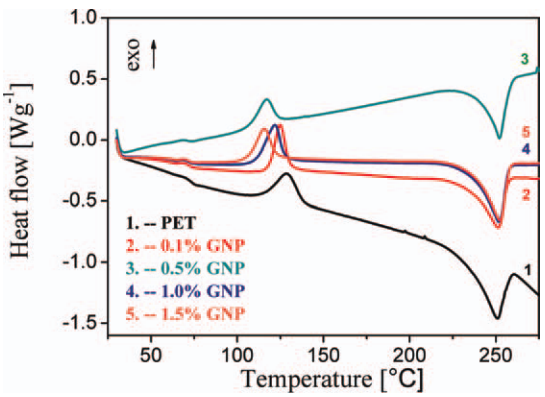

Figure 3. First heating scans of neat PET and PET/GNPs nanocomposites. [Color figure can be viewed in the online issue, which is available at wileyonlinelibrary.com.]

Table II. DSC Characterization of the Materials Used, Calculated from the First Heating Scans

Material	T_g (°C)	T_{cc} (°C)	T_m (°C)	T_c (°C)
PET (Ref.)	73	129	250	216
0.1% GNP	72	125	251	216
0.5% GNP	72	117	252	215
1.0% GNP	72	122	251	211
1.5% GNP	72	116	252	216

Table III. TGA Data of Neat PET and PET/GNPs Nanocomposites

Material	T (°C) 10% loss	T_d (°C)	Residue @ 600°C (%)
PET (Ref.)	401	434	11.4
0.1% GNP	403	433	11.6
0.5% GNP	407	437	15.4
1.0% GNP	407	432	16.4
1.5% GNP	412	435	16.5

with the assumption that GNPs behave as nucleating agents as a result of their large relative surface area. Because graphite sheets have an adsorption effect on PET molecules, the movement of macromolecules is restricted, and PET molecules are more readily nucleated heterogeneously.[34–38] As a result, PET/GNP compositions crystallize at lower temperatures during the heating process. However, as seen from the T_c values, this effect is unnoticeable during the cooling process, probably because homogenous nucleation from the melt of PET is spontaneous.

The glass transition temperature, T_g, is identified as a change in the heat capacity of the sample (the baseline of the DSC trace), marked by the shoulder at ~72°C. The T_g values in Table II, calculated from the inflection point of the transition, do not exhibit a significant GNP effect.

The thermal stability (under nitrogen) of the different compositions was determined by TGA; the respective traces are shown in Figure 4 and the corresponding thermal stability data are displayed in Table III. The sample weight loss curves show that, in all the cases, degradation occurs in one step from 400 to 500°C. This process is attributed to scission of the main chain, with the evolution of low molecular weight species, resulting in the observed weight loss. It appears that degradation occurs in a manner similar to that of pure PET, regardless of the presence of GPNs, whose contribution seems to be negligible despite the fact that their thermal stability is very high, with only little weight loss up to 800°C.[39]

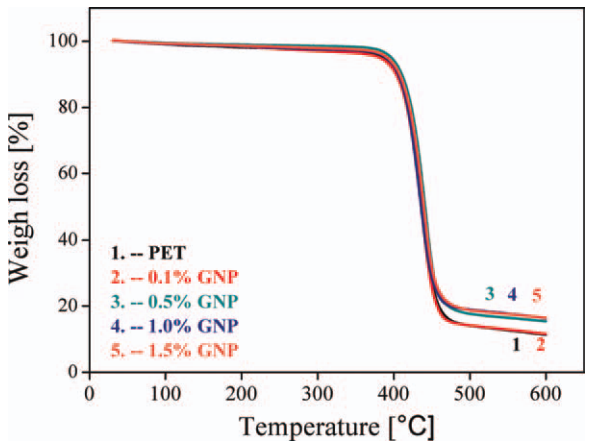

Figure 4. Thermal gravimetric analyses of neat PET and PET/GNPs nanocomposites. [Color figure can be viewed in the online issue, which is available at wileyonlinelibrary.com.]

Although the effect of GNP can hardly be detected and the degradation temperature T_d (defined as the inflection point in the TGA trace) is seemingly unaffected in a consistent manner, two minimal differences can be distinguished, namely, the temperature at 10% weight loss and the weight residue at 600°C. Both observations suggest that GNP stabilizes the PET—manifested in delaying its degradation by 10 K and in increasing its char residue by 5 wt % at 1.5 wt % GNP content. This distinct improvement in thermal stability of the nanocomposites can be associated with the two-dimensional planar structure of dispersed GNPs in the PET matrix, which serve as barriers by forming a tortuous path for the degradation products. This behavior is analogous to that of layered clay on flame retardance of polymers.[40]

Considering the char residue, a similar behavior was reported for epoxy/graphite platelets.[41] Thus, PET/GNPs nanocomposites have a somewhat better thermal stability compared with that of pure PET.

Characterization of the Dispersion

The quality of the dispersion of the nanoparticles in the polymer is clearly known to influence the two main factors that in turn affect permeability. The inherent barrier contribution of the nanoparticles and the crystallinity of the polymer. Here, qualitative characterization was obtained through the study of fracture surfaces of the PET/GNP films. Figure 5 presents relatively low-magnification SEM micrographs of two PET/GNP compositions. Figure 5(a) shows the full thickness of a film (1.0 wt % GNP); a number of GNP flakes can be seen protruding from the surface. Figure 5(b,c) present films with a slightly higher GNP concentration (1.5 wt %) at a higher magnification; the arrows indicate several clearly identified GNPs. Two observations are apparent: First, the GNPs are by and large individually dispersed and exfoliated—with no indication of aggregates. Second, the long axis of the processed GNP flakes lies parallel to the plane of the film.

Mechanical Properties

Table IV shows the tensile properties of the materials used. It is apparent that in the presence of GNPs, the Elastic modulus (E) of PET was greater than that of neat PET throughout all the content range, within an acceptable standard deviation. This is typical for inorganic filled composites.[42] The maximum E for PET/GNPs was observed at 1.5 wt %, where it increased from 1.16 GPa (neat PET) to 1.40 GPa. This increase in the modulus even at low GNP concentrations is consistent with that of other polymers containing fillers of nanometric size.[43,44] This increase may

originate from both the presence of stiff graphite particles and a graphite-induced increase in the degree of crystallinity of PET.

While the Young's modulus of PET/GNP increased with subsequent additions of GNPs, it was found that the elongation at break and the tensile strength decreased by some 40 and 56%, respectively, with the incorporation of 1.5 wt % GNPs.[45]

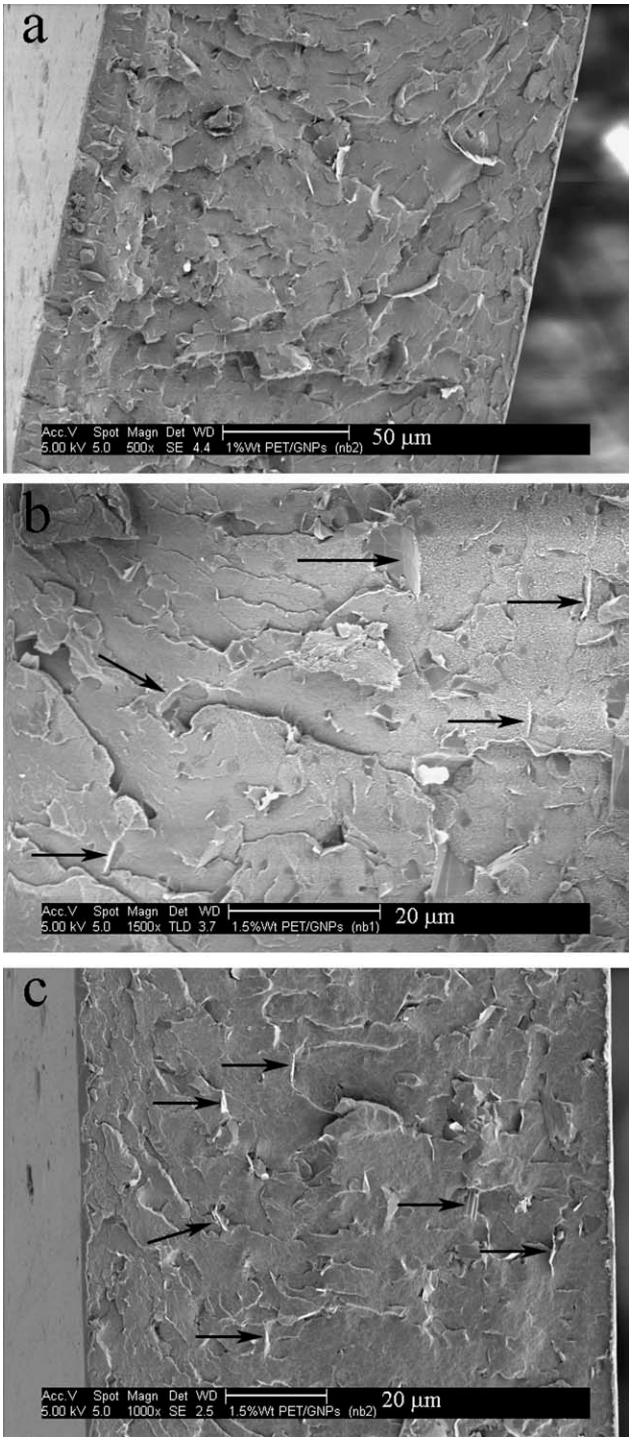

Figure 5. Scanning electron micrographs of fractured surfaces of PET/GNPs films: (a) PET/1% GNP film; (b, c) PET/1.5% GNP film in higher magnification, the arrows pointing at part of the GNP nanoparticles.

Table IV. Tensile Properties of Neat PET and PET/GNPs Nanocomposites

Material	Max. stress (MPa)	Max. strain (%)	*E* (GPa)
PET (Ref.)	53.82 ± 9.48	7.72 ± 1.30	1.16 ± 0.14
0.1% GNP	47.99 ± 3.03	5.25 ± 0.73	1.17 ± 0.05
0.5% GNP	39.50 ± 7.76	4.31 ± 1.51	1.21 ± 0.14
1.0% GNP	35.39 ± 10.00	3.43 ± 1.55	1.36 ± 0.06
1.5% GNP	30.21 ± 8.11	3.11 ± 1.61	1.40 ± 0.02

CONCLUSIONS

The oxygen barrier properties of PET are improved immensely through the addition of graphite nanoplatelets. In the best case, an addition of 1.5 wt % of GNPs reduced the oxygen transmission rate value of a nanocomposite film (with a degree of crystallinity $X_c = 17.3\%$) from 11.1 to 0.1 cc/m^2/day/atm, compared with the neat PET control. The potential of the PET/GNP films in oxygen barrier applications to outperform those of neat PET is noticeably evident and in the best case, for 1.5 wt % GNP, the oxygen permeation was reduced by more than 99%. The mechanism that generates this effect is related to two factors: The first is the inherent barrier property of the dispersed GNPs, whose presence in the polymer increases the path for the diffusing molecules (tortuosity); the second is the higher degree of crystallinity nucleated by GNPs in the polymer. As this research indicates, the processing conditions governing the quality of the dispersion and the polymer crystallinity and morphology should be considered together in order to optimize the final materials' properties.

The improved barrier properties due to GNP are accompanied by an advantageous higher dimensional stability, linked to the stiffening effect of the GNPs, and by improved thermal stability. Yet, the presence of GNPs in the polymer results in lower strengths and greater brittleness. For the best performance requirements, an optimized composition and processing conditions can be selected for minimum oxygen transmission and high dimensional stability with maximum strength retention.

REFERENCES

1. Bandi, S.; Mehta, S.; Schiraldi, D. A. *Polym. Degrad. Stab.* **2005,** *88*, 341.
2. Doudou, B. B.; Dargent, E.; Grenet, J. J. *J. Plast. Film Sheet.* **2005,** *21*, 233.
3. Hu, Y. S.; Prattipati, V.; Mehta, S.; Schiraldi, D. A.; Hiltner, A.; Baer, E. *Polymer* **2005,** *46*, 2685.
4. Bashir, Z.; Al-Aloush, I.; Al-Raqibah, I.; Ibrahim, M. *Polym. Eng. Sci.* **2000,** *40*, 2442.
5. Sekelik, D. J.; Stepanov, E. V.; Nazarenko, S.; Schiraldi, D.; Hiltner, A.; Baer, E. *J. Polym. Sci. Pt. B-Polym. Phys.* **1999,** *37*, 847.
6. Polyakova, A.; Stepanov, E. V.; Sekelik, D.; Schiraldi, D. A.; Hiltner, A.; Baer, E. *J. Polym. Sci. Pt. B-Polym. Phys.* **2001,** *39*, 1911.
7. Lin, J.; Shenogin, S.; Nazarenko, S. *Polymer* **2002,** *43*, 4733.

8. Liu, R. Y. F.; Schiraldi, D. A.; Hiltner, A.; Baer, E. *J. Polym. Sci. Pt. B-Polym. Phys.* **2002,** *40*, 862.
9. Liu, R. Y. F.; Hiltner, A.; Baer, E. *J. Polym. Sci. Pt. B-Polym. Phys.* **2004,** *42*, 493.
10. Bornschlegl, E.; Bonart, R. *Colloid Polym. Sci.* **1980,** *258*, 319.
11. Pixton, M. R.; Paul, D. R. In Polymeric Gas Separation Membranes; Paul, D. R.; Yampol'skii, Yu. P., Eds.; CRC: Boca Raton, FL, **1994;** Chapter 3, p 83.
12. Aitken, C. L.; Koros, W. J.; Paul, D. R. *Macromolecules* **1992,** *25*, 3424.
13. Sykes, G. F.; St. Clair, A. K. *J. Appl. Polym. Sci.* **1986,** *32*, 3725.
14. Stern, S. A.; Mi, Y.; Yamamoto, H. *J. Polym. Sci. Pt. B-Polym. Phys.* **1989,** *27*, 1887.
15. Tanaka, K.; Kita, H.; Okamoto, K.; Nakamura, A.; Kusuki, Y. *Polym. J.* **1990,** *22*, 381.
16. Coleman, M. R.; Koros, W. J. *J. Membr. Sci.* **1990,** *50*, 285.
17. Light, R. R.; Seymour, R. W. *Polym. Eng. Sci.* **1982,** *22*, 857.
18. Sheu, F. R.; Chern, R. T. *J. Polym. Sci. Pt. B-Polym. Phys.* **1989,** *27*, 1121.
19. Lee, H.-J.; Oh, S.-J.; Choi, J.-Y.; Kim, J. W.; Han, J.; Tan, L.-S.; Baek, J.-B. *Chem. Mater.* **2005,** *17*, 5057.
20. Gomez-del Rio, T.; Poza, P.; Rodriguez, J.; Garcia-Gutierrez, M. C.; Hernandez, J. J.; Ezquerra, T. A. *Compos. Sci. Technol.* **2010,** *70*, 284.
21. Zhang, M..; Li, D.-J.; Wu, D.-F.; Yan, C.-H.; Lu, P.; Qiu, G.-M. *J. Appl. Polym. Sci.* **2008,** *108*, 1482.
22. Zhang, H.-B.; Zheng, W.-G.; Yan, Q.; Yang, Y.; Wang, J.-W.; Lu, Z.-H.; Ji, G.-Y.; Yu, Z.-Z. *Polymer* **2010,** *51*, 1191.
23. Li, M.; Jeong, Y. G. *Compos. Part A: Appl. Sci. Manuf.* **2011,** *42*, 560.
24. Bandla, S.; Hanan J. C. *J. Mater. Sci.* **2012,** *47*, 876.
25. Paul, D. R.; Robeson, L. M. *Polymer* **2008,** *49*, 3187.
26. Hwang, S. Y.; Lee, W. D.; Lim, J. S.; Park, K. H.; Im, S. S. *J. Polym. Sci. Pt. B-Polym. Phys.* **2008,** *46*, 1022.
27. Ji, Q.; Wang, X. L.; Zhang, Y. H.; Kong, Q. S.; Xia, Y. Z. *Compos. Pt. A-Appl. Sci. Manuf.* **2009,** *40*, 878.
28. Kim, H.; Abdala, A.; Macosko, C. W. *Macromolecules* **2010,** *43*, 6515.
29. Li, J.; Kim, J. K.; Sham, M. L. *Scripta Mater.* **2005,** *53*, 235.
30. Li, J.; Vaisman, L.; Marom, G.; Kim, J. K. *Carbon* **2007,** *45*, 744.
31. Jog, J. P. *J. Macromol. Sci. Part C-Polym. Rev.* **1995,** *35*, 531.
32. Kalaitzidou, K.; Fukushima, H.; Drzal, L. T. *Carbon* **2007,** *45*, 1446.
33. Cussler, E. L.; Hughes, S. E.; Ward, W. J., III; Aris, R. *J. Membr. Sci.* **1988,** *38*, 161.
34. Prattipati, V.; Hu, Y. S.; Bandi, S.; Schiraldi, D. A.; Hiltner, A.; Baer, E.; Mehta, S. *J. Appl. Polym. Sci.* **2005,** *97*, 1361.
35. Nadkarni, V. M.; Shingankuli, V. L.; Jog, J. G. *Polym. Eng. Sci.* **1988,** *28*, 1326.
36. Kamal, M. R.; Sahto, M. A.; Utracki, L. A. *Polym. Eng. Sci.* **1982,** *22*, 1127.
37. Varma, D. S.; Dhar, V. K. *J. Appl. Polym. Sci.* **1987,** *33*, 1103.
38. Tanrattanakul, V.; Hiltner, A.; Baer, E.; Perkins, W. G.; Massey, F. L.; Moet, A. *Polymer* **1997,** *38*, 2191.
39. Kim, I.-H.; Jeong, Y. G. *J. Polym. Sci. Pt. B-Polym. Phys.* **2010,** *48*, 850.
40. Frounchi, M.; Dourbash, A. *Macromol. Mater. Eng.* **2009,** *294*, 68.
41. Yasmin, A.; Daniel, I. M. *Polymer* **2004,** *45*, 8211.
42. Matsuo, Y.; Hatase, K.; Sugie, Y. *Chem. Mater.* **1998,** *10*, 2266.
43. Zheng, W.; Wong, S.-C. *Compos. Sci. Technol.* **2003,** *63*, 225.
44. Alexandre, M.; Dubois, P. *Mater. Sci. Eng. R Rep.* **2000,** *28*, 1.
45. Corcione, C. E.; Cavallo, A.; Pesce, E.; Greco, A.; Maffezzoli, A. *Polym. Eng. Sci.* **2011,** *51*, 1280.